High-Capacity Angularly Multiplexed Holographic Memory Operating at the Single-Photon Level

Radosław Chrapkiewicz,[1] Michał Dąbrowski,[1,*] and Wojciech Wasilewski[1]
Institute of Experimental Physics, Faculty of Physics, University of Warsaw, Pasteura 5, 02-093 Warsaw, Poland
(Received 20 April 2016; published 8 February 2017)

We experimentally demonstrate an angularly multiplexed holographic memory capable of intrinsic generation, storage, and retrieval of multiple photons, based on an off-resonant Raman interaction in warm rubidium-87 vapors. The memory capacity of up to 60 independent atomic spin-wave modes is evidenced by analyzing angular distributions of coincidences between Stokes and time-delayed anti-Stokes light, observed down to the level of single spin-wave excitation during the several-microsecond memory lifetime. We also propose how to practically enhance rates of single- and multiple-photon generation by combining our multimode emissive memory with existing fast optical switches.

DOI: 10.1103/PhysRevLett.118.063603

The construction of on-demand sources of desired quantum states of light remains an overarching goal for quantum engineering. While single photons are an essential resource for quantum communication protocols [1,2], multiple-photon states offer an avenue for quantum computing with linear optics [3,4] and quantum simulations, e.g., in boson sampling schemes [5,6]. Since scientists are already able to manufacture complex photonic chips using femtosecond writing technologies [7], perhaps the last major roadblock to perform linear-optics simulations unattainable by classical computing is the ability to create a large number of photons capable of nonclassical interference [8].

Prospective solutions to achieve this nontrivial, long-standing goal rely on still developing quantum dot sources [9–11] and a Rydberg blockade [12,13] as well as parametric processes such as four-wave mixing [14] and spontaneous parametric down-conversion (SPDC) routinely employed to produce heralded single photons [15]. The present technology of SPDC sources is well developed and widespread, since, while operating in room temperatures, it offers high brightness and renders low noise. Nonetheless, the intrinsic feature of parametric sources is their purely stochastic operation. The probability of photon pair generation must be kept low to suppress the contribution of higher numbers of photons. A possible way to surpass this stochastic behavior is to combine multiple sources with fast, active optical switches [16,17] to increase the chances for single-photon generation. In practice, setups with at most four sources using SPDC [18,19] and 12 sources with cold atoms [20] have been demonstrated. Furthermore, N parametric sources can be used to generate N heralded photons, but this method requires a very long waiting time [18] as the probability for N-photon state generation falls exponentially with N.

Recently, Nunn *et al.* [21] have suggested a possible solution for the enhanced generation of N-photon states in a system with N quantum memories storing heralded photons from N independent SPDC sources and releasing them at once. Here we present a different approach, where photons can be generated directly inside many emissive quantum memories driven by a Raman scattering process where the deposition of an excitation is heralded by a detection of a Stokes photon. Moreover, as depicted in Figs. 1(a)–1(c), multiple memories are implemented in our experiment within one atomic ensemble, which serves as a single holographic memory interfacing many overlapping spin-wave modes of different spatial periodicity with independent angular modes of light. The presented angular multiplexing of many modes provides a tremendous simplification of experimental setups as compared to hypothetical multiple stand-alone memory systems.

Similarly as in SPDC sources, the probability ζ of generating a single excitation in any of the memory modes has to be low, to suppress the probability ζ^2 for generating two excitations. However, if the number of available emissive modes M is large, the probability of photon generation in at least one of them $1-(1-\zeta)^M$ can approach unity [17]. For instance, for $\zeta = 10^{-2}$, $M = 100$, the probability for Stokes photon generation reaches 60%. Once a photon is emitted in any of M modes, one can use an active optical switch [16,17] seeded by a triggering signal from the Stokes scattering to route the anti-Stokes photon to a desired single output, as illustrated in Fig. 1(d). Such an operation essentially relies on a memory storage time which has to exceed the nanoseconds-long reconfiguration time of the optical switch [16,17].

Note that the probability for M modes to generate exactly N photons $\binom{M}{N}\zeta^N(1-\zeta)^{M-N}$ can also be high. For $N = 8$, $M = 100$, it reaches a value of 7×10^{-6}, which is over 10 orders of magnitude larger than the probability to obtain eight photons from eight independent sources $\zeta^8 = 10^{-16}$. The scheme of Fig. 1(d) could be upgraded with a multiple-outputs switch. This way, after each successful generation of N excitations, the same multiphoton state of the product form

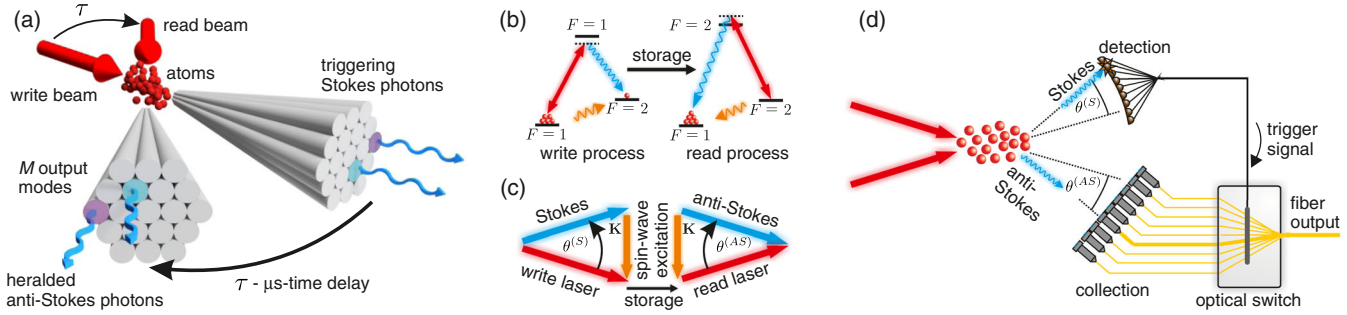

FIG. 1. (a) Idea of holographic memory generating, storing, and releasing on-demand angularly correlated photons. Photons are produced in $2 \times M$ modes which are pairwise coupled. In each independent pair of modes (e.g., colored circles), anti-Stokes photons are heralded by Stokes photons generation, with microsecond-time delay advance. (b) The generation and retrieval of photons is performed in a Raman scattering process, using Λ-system ^{87}Rb energy levels. (c) The phase-matching condition relates wave vectors of driving laser beams, photons, and spin-wave excitation and determines the scattering angle of an anti-Stokes photon $\boldsymbol{\theta}^{(\mathrm{AS})} \simeq -\boldsymbol{\theta}^{(\mathrm{S})}$. (d) The predictability of the scattering angles of anti-Stokes photons can be utilized to match outgoing photons to an optical switch [16,17] with one or multiple outputs (not shown). The switch architecture is reconfigured after the detection of the Stokes trigger photons so as to pass single or N photons into the desired fiber links.

$|1\rangle \otimes \cdots \otimes |1\rangle$ can be produced in a desired set of output fibers. Most of the elements of this scheme such as matrices of single-photon detectors, fiber bundles, and fast optical switches have been demonstrated or are commercially available. The centerpiece is the multiplexed source of heralded photons with a sufficient time delay, based on spatial [20], temporal [22,23], or another degree of freedom.

In this Letter, we experimentally demonstrate a holographic atomic memory that can generate, store, and retrieve light at the single-photon level in many independent angular modes whose number could practically reach thousands [24] under realistic experimental conditions. Rather than using external nondeterministic sources of spectrally filtered, heralded photons to convert them to atomic collective excitations [25], the Stokes photon generated inside the memory heralds the spin-wave creation which can be retrieved on demand in the time-delayed anti-Stokes scattering process. The combination of a large number of emissive modes with predictability offered by a memory time delay can circumvent the limits of SPDC sources and serve as an enhanced-rate source of photons. Moreover, our approach bridges the gap between numerous experiments with warm atomic memories with a single spatial mode of light at the single-photon level [25–28] and a few spatially multimode experiments performed at macroscopic light levels [29,30].

The operation of our memory presented in Figs. 1(a)–1(c) relies on collective multimode Raman scattering in atomic vapors in a Duan-Lukin-Cirac-Zoller scheme [1]. The angular correlations between Stokes and anti-Stokes photons, mediated by the phase-matching conditions depicted in Fig. 1(c), arise in a way similar to holography [31]. First, we write to the memory by driving a spontaneous Raman transition in the Λ system, producing pairs of collective atomic excitation and spontaneous Stokes photons scattered in random directions. The write process resembles the registering of a hologram, and, depending on the Stokes photon scattering angle $\boldsymbol{\theta}^{(\mathrm{S})}$, the spin wave with the wave vector $\mathbf{K} = 2\pi\boldsymbol{\theta}^{(\mathrm{S})}/\lambda$ is created, where λ stands for a wavelength of a driving beam. Then, after adjustable storage time τ, the atomic excitation can be converted to an anti-Stokes photon with up to $\eta_{\mathrm{read}} = 30\%$ internal read efficiency [27,32,33]. The read process is analogous to the reconstruction of a hologram, and the angle of the anti-Stokes photon emission $\boldsymbol{\theta}^{(\mathrm{AS})} \simeq -\boldsymbol{\theta}^{(\mathrm{S})}$ is determined by the preceding detection of the Stokes photon direction, a few microseconds in advance. Remarkably, the holographic storage allows us to populate, store, and retrieve multiple overlapping yet independent spin-wave modes in the same ensemble of atoms.

The simplified scheme of the experimental setup is depicted in Fig. 2 (cf. [41,42] for details). We pump atoms into $5^2S_{1/2}$, $F = 1$ and drive the Raman transition to the $5^2S_{1/2}$, $F = 2$ level. The driving laser detuning was approximately 700 MHz from $5^2P_{1/2}$, $F = 1$ or $5^2P_{3/2}$, $F = 2$ levels as marked in Fig. 1(b). The main glass cell of $L = 10$ cm length was filled with ^{87}Rb mixed with krypton at 1 Torr and heated to 60°–75 °C corresponding to optical depths (OD) from 50 up to 80. The $1/e^2$ diameters of the linearly polarized driving beams at 795 or 780 nm tilted by 10 mrad inside the cell were about $2w = 4.6$ mm, while the pump beam at 780 nm was twice as large. The typical experimental sequence depicted in the inset in Fig. 2 consists of pulses of 70 mW pump, 20 mW write, and 15 mW read laser of duration $t_p \approx 1$ ms, $t_w \simeq t_r \approx 1$ μs, while the storage period is varied in the range $0 \leq \tau \leq 40$ μs. The triple filtering system—Wollaston prism, atomic absorption filter, and Faraday filter (cf. [42] for details)—is used to perform coincidence measurements at the single-photon level. The essential advantage of our solution over routine spectral filtering

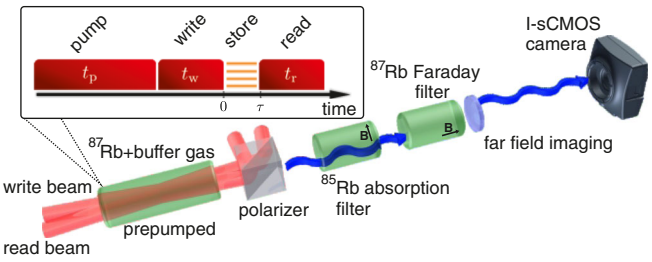

FIG. 2. The simplified scheme presenting key parts of the experimental setup for the holographic memory. The generation and storage of photons are implemented in warm ^{87}Rb vapors whose thermal motion is slowed down by an admixture of noble buffer gas. Inset: Experimental sequence. The triple filtering system [42] (polarization and two-step spectral; **B** denotes the magnetic field vector) passes scattered photons at different angles and blocks all laser beams detuned by 6.8 GHz. The detection of photons with a high angular resolution is performed with an I-sCMOS camera capable of resolving photon coincidences [33,43].

using Fabry-Perot interferometers is its transmission being insensitive to a photon scattering angle. We obtain a large transmission of ca. 50% for both Stokes and anti-Stokes photons while attenuating 6.8 GHz detuned driving beams by the factor of 10^{11}. Moreover, narrow spectral windows of the Faraday filter suppress the broadband collisional fluorescence [26] by at least 2 orders of magnitude and virtually block the contribution from the four-wave mixing during the read process [32]. Finally, we split Stokes from anti-Stokes using interference filters and angularly resolve them with suitable focusing lenses. Each field is directed to a separate region on the intensified scientific CMOS (I-sCMOS) camera [33,43,44] used for counting coincidences.

Example, raw single-shot images of the Stokes and the 500-ns-delayed anti-Stokes scattering are presented in Fig. 3(a). Visibly separated spots originate from multiple Raman scattered photons impinging the camera image intensifier where they are converted to bright phosphor flashes. The registered photons are noticeably grouped in specklelike patterns [41], which in the anti-Stokes process are angularly inverted as compared to the Stokes scattering, following the phase-matching condition in Fig. 1(c). Here we exemplify an outcome of a high-gain Raman process where hundreds of photons are scattered in each shot, for $t_w = 2\ \mu$s, $t_r = 1\ \mu$s, and OD = 80. Thereafter, we decreased the number of Stokes scattered photons whose mean number depends exponentially (high gain) on write pulse duration t_w and OD. From each captured frame, we extract the coordinates of individual photon detection events $\boldsymbol{\theta}^{(\mathrm{S})} = (\theta_x^{(\mathrm{S})}, \theta_y^{(\mathrm{S})})$ and $\boldsymbol{\theta}^{(\mathrm{AS})} = (\theta_x^{(\mathrm{AS})}, \theta_y^{(\mathrm{AS})})$ for the Stokes and anti-Stokes separate camera regions, respectively, with a real-time software processing [43,44] as visualized in Fig. 3(b). An example processed frame in the low-gain regime for $t_w = 250$ ns, $t_r = 500$ ns, and OD = 50 is shown in Fig. 3(c).

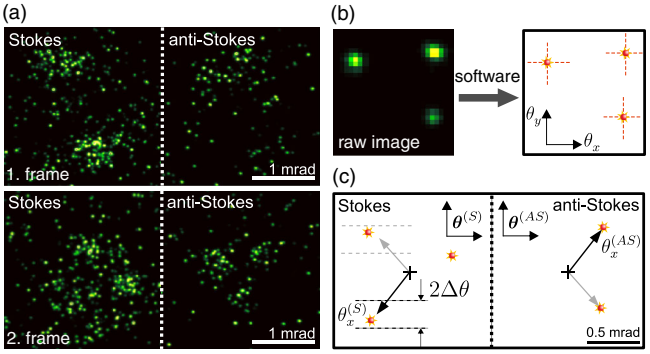

FIG. 3. (a) Two example cropped frames with Stokes and 500-ns-delayed anti-Stokes photons detected as bright spots on the I-sCMOS camera. Hundreds of angularly resolved photons from a high-gain Raman scattering form pairwise inverted random patterns. (b) A real-time software algorithm converts with subpixel resolution raw I-sCMOS images into sets of coordinates representing central positions of individual single-photon spots [43]. (c) An example processed frame with several photons scattered in a low-gain regime. We further accumulate histograms of photon coordinates $n_{\mathrm{coinc}}(\theta_x^{(\mathrm{S})}, \theta_x^{(\mathrm{AS})})$ for coincidences where a detected anti-Stokes photon was preceded by a Stokes trigger found in a stripe fulfilling the phase-matching condition $\theta_y^{(\mathrm{S})} = -\theta_y^{(\mathrm{AS})} \pm \Delta\theta$, where $\Delta\theta = 0.15$ or 0.3 mrad. Black crosses mark driving beam directions.

We quantify the angular properties of the Raman scattering by measuring and analyzing distributions of coincidences $n_{\mathrm{coinc}}(\boldsymbol{\theta}^{(\mathrm{S})}, \boldsymbol{\theta}^{(\mathrm{AS})})$ between the Stokes and time-delayed anti-Stokes photons. To confirm the angular correlations between time-delayed photons $\boldsymbol{\theta}^{(\mathrm{AS})} \simeq -\boldsymbol{\theta}^{(\mathrm{S})}$, it is convenient to display and focus on bidimensional coincidence distributions such as $n_{\mathrm{coinc}}(\theta_x^{(\mathrm{S})}, \theta_x^{(\mathrm{AS})})$, equivalent to a measurement with two one-dimensional detectors; cf. [45]. As illustrated in Fig. 3(c), to utilize all photons detected in two-dimensional camera frames, we take into account photon pairs that appear in conjugate θ_y-separated stripes such $|\theta_y^{(\mathrm{S})} + \theta_y^{(\mathrm{AS})}| < \Delta\theta$, integrating over $\theta_y^{(\mathrm{S})}$, $\theta_y^{(\mathrm{AS})}$ coordinates:

$$n_2(\theta_x^{(\mathrm{S})}, \theta_x^{(\mathrm{AS})}) = \int d\theta_y^{(\mathrm{AS})} \int_{\theta_y^{(\mathrm{AS})}-\Delta\theta}^{\theta_y^{(\mathrm{AS})}+\Delta\theta} d\theta_y^{(\mathrm{S})} n_2(\boldsymbol{\theta}^{(\mathrm{S})}, \boldsymbol{\theta}^{(\mathrm{AS})}). \tag{1}$$

The total number of coincidences counted this way, $n_2(\theta_x^{(\mathrm{S})}, \theta_x^{(\mathrm{AS})})$, is a sum of two factors: the total number of Stokes– anti-Stokes pairs $n_{\mathrm{coinc}}(\theta_x^{(\mathrm{S})}, \theta_x^{(\mathrm{AS})})$ and accidental coincidences from uncorrelated noise $n_{\mathrm{acc}}(\theta_x^{(\mathrm{S})}, \theta_x^{(\mathrm{AS})})$ whose spatial distribution reads as follows:

$$n_{\mathrm{acc}}(\theta_x^{(\mathrm{S})}, \theta_x^{(\mathrm{AS})}) = \frac{1}{\mathcal{N}} \int d\theta_y^{(\mathrm{AS})} \times \int_{\theta_y^{(\mathrm{AS})}-\Delta\theta}^{\theta_y^{(\mathrm{AS})}+\Delta\theta} d\theta_y^{(\mathrm{S})} n_1(\boldsymbol{\theta}^{(\mathrm{S})}) n_1(\boldsymbol{\theta}^{(\mathrm{AS})}), \tag{2}$$

where $n_1(\boldsymbol{\theta}^{(\mathrm{S})})$ and $n_1(\boldsymbol{\theta}^{(\mathrm{AS})})$ are distributions of the number of photons collected in both camera regions and $\mathcal{N}$ is the total number of frames. Therefore, the number of Stokes–anti-Stokes pairs can be calculated by subtracting Eq. (2) from Eq. (1) [45]. At the center of the distribution, the accidental coincidences constitute about 58% of the total number of pairs.

In Fig. 4(a), we present histograms representing the angular distribution of coincidences between Stokes and anti-Stokes photons $n_{\mathrm{coinc}}(\theta_x^{(\mathrm{S})}, \theta_x^{(\mathrm{AS})})$ for three different storage times $\tau = 0.5, 3.5, 5.5\ \mu$s, each obtained from 3×10^5 frames for $t_w = 1\ \mu$s, $t_r = 1\ \mu$s, and $\mathrm{OD} = 80$, for a high Raman gain ($\eta_{\mathrm{read}} = 30\%$). The maximum number of Stokes–anti-Stokes generated pairs per mode per single shot translates here to about 40 after correcting for the setup transmission and the detection efficiency. The characteristic elongated antidiagonal shapes attest to the conjugation of opposite angles of Stokes and time-delayed anti-Stokes scattering resulting from the phase-matching condition $\theta_x^{(\mathrm{AS})} \simeq -\theta_x^{(\mathrm{S})}$. The diagonal $1/e^2$ width of $2w_{\mathrm{corr}} = 1.2$ mrad, almost independent of a storage time, represents the angular spread of the mode of anti-Stokes emission conditioned on the preceding Stokes localization. The antidiagonal width $2w_{\mathrm{avg}}$ represents a span of angles $\theta_x^{(\mathrm{AS})}$ where the anti-Stokes light is detected. It decreases during storage due to the diffusion of atoms in the buffer gas [30,46], which in turn washes out dense fringes in the stored spin-hologram coupling to higher angles of scattering [33].

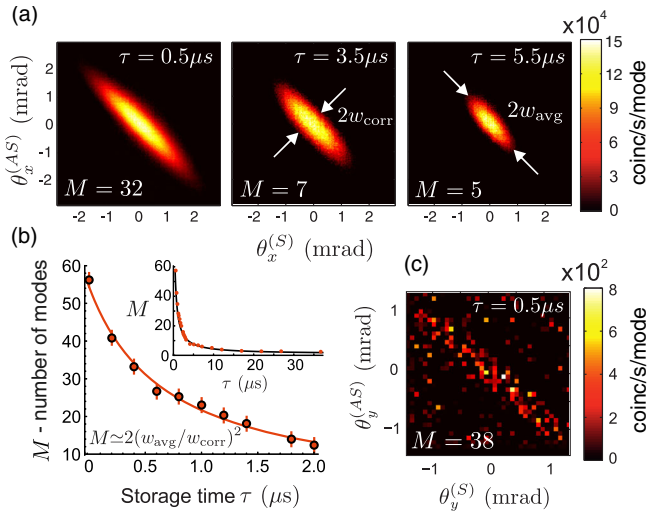

FIG. 4. (a) Angular distributions of Stokes and anti-Stokes photon coincidences $n_{\mathrm{coinc}}(\theta_x^{(\mathrm{S})}, \theta_x^{(\mathrm{AS})})$ for increasing storage times τ reveal angular correlations $\theta_x^{(\mathrm{AS})} \simeq -\theta_x^{(\mathrm{S})}$ between photons stored and retrieved from the holographic memory. A visible decay of high-scattering-angle events is determined by a diffusional decoherence [46]. (b) A doubled squared ratio between the antidiagonal and diagonal width of coincidence histograms is used to estimate the total number of retrieved angular modes $M < 60 \simeq \mathcal{F}$ versus the storage time in agreement with the diffusion model [33]. Tens of modes are retrieved within the first 2 μs, which is sufficiently long to couple the holographic memory source with currently existing optical switches [16,17] [cf. Fig. 1(d)]. Inset: A few modes can be retrieved in up to tens of microseconds. (c) Coincidences are observable down to the single spin-wave excitation level.

The estimated number of modes M of our memory can be taken as the ratio of the solid angle span of anti-Stokes to a single mode spread $M \simeq 2(w_{\mathrm{avg}}/w_{\mathrm{corr}})^2$ [41], taking into account the full two-dimensional mode structure illustrated in Fig. 1(a). We calculate the number of modes M on the respective coincidence distributions, and in Fig. 4(b), we present its dependence on the storage time acquired from additional measurement series, together with curve fitting [33]. M dropped from 58 for an instantaneous retrieval to 12 after 2 μs storage time. In the inset, we can observe that for longer storage times the number of retrieved modes drops to 2 within about 20 μs. The maximum value displayed in Fig. 4(b) is close to the Fresnel number of the atomic ensemble $\mathcal{F} = w^2/\lambda L \approx 66$ as can be expected from the theory $M \simeq \mathcal{F}$ [47]. We therefore envisage that, by increasing the beam diameter about 4 times up to 18 mm, the retrieval of even 1000 modes should be realistic.

Finally, in Fig. 4(c), we demonstrate the operation of the memory at the single excitation level, where the maximum number of pairs generated per shot per mode is about 5×10^{-2}, for $t_w = 250$ ns, $t_r = 500$ ns, and $\mathrm{OD} = 50$ providing a low Raman gain ($\eta_{\mathrm{read}} = 13\%$). Here the coincidence distribution $n_{\mathrm{coinc}}(\theta_y^{(\mathrm{S})}, \theta_y^{(\mathrm{AS})})$ acquired from 10^6 frames reveals a similar structure and consequently the number of retrieved modes M as in the higher gain regime. By keeping the probability for photon pair per mode low, here we generate on average ca. 0.9 Stokes–anti-Stokes pairs per shot in the whole memory [33]. This is evidence of a possible rate enhancement due to the mode multiplexing, while photons are 0.5 μs delayed in time.

In both the high- and low-gain regimes, we obtain the ratio of coincidences to overall registered pairs of approximately 42%, which is comparable with single-spatial-mode warm atomic memories [25,27,28]. The noise of the same frequency as anti-Stokes photons originates primarily from collisions with a buffer gas [48] that lead to isotropic and incoherent Stokes scattering in the read stage. Although an employment of even more stringent spectral filtering would further decrease a broadband noise component as shown in a single-spatial-mode system [28], we suspect that further demonstrations beyond proof of principle, aiming in a practical N-photon source, may benefit from implementations in cold atomic systems where high nonclassical correlations can be readily achieved [49–51].

In conclusion, we presented the first experimental demonstration of a large number of angular modes from the emissive atomic memory that predictably generate anti-Stokes photons in a direction known several microseconds in advance through the preceding detection of Stokes photons. In our implementation in warm rubidium-87

vapors, we were generating, storing, and retrieving light at the single-photon level from up to 60 spin-wave modes whose number can be further scaled up with an increasing Fresnel number [24,47]. From supporting measurements, we infer that no more than one spin wave per mode is present in the memory [33], but nonclassical operation of the memory is not directly shown. We suggest that a combination of such multimode memory with existing optical switches [16,17] will be a realistic method for enhanced-rate generation of single- [52,53] or N-photon states, the latter being a prerequisite for linear-optics quantum computing [3,4] and simulations [5,6]. Our work constitutes the first observation of time-delayed multimode angular correlations at the single-photon level in contrast to all previous studies, where such correlations were observed exclusively in instantaneous nonlinear processes [54], such as parametric down-conversion [55] or four-wave mixing [56].

We acknowledge discussions with A. Bogucki, M. Jachura, A. Leszczyński, M. Lipka, M. Mazelanik, M. Parniak, and P. Ziń as well as the support of K. Banaszek and J. Iwaszkiewicz. This project was financed by the National Science Center (Poland) (Grants No. DEC-2011/03/D/ST2/01941 and No. DEC-2015/19/N/ST2/01671) and PhoQuS@UW (Grant Agreement No. 316244), and it was supported in part by PL-Grid Infrastructure. R. C. was supported by the Foundation for Polish Science.

*mdabrowski@fuw.edu.pl

[1] L.-M. Duan, M. D. Lukin, J. I. Cirac, and P. Zoller, Nature (London) **414**, 413 (2001).
[2] Z.-S. Yuan, Y.-A. Chen, B. Zhao, S. Chen, J. Schmiedmayer, and J.-W. Pan, Nature (London) **454**, 1098 (2008).
[3] E. Knill, R. Laflamme, and G. J. Milburn, Nature (London) **409**, 46 (2001).
[4] P. Kok, W. J. Munro, K. Nemoto, T. C. Ralph, J. P. Dowling, and G. J. Milburn, Rev. Mod. Phys. **79**, 135 (2007).
[5] A. Peruzzo *et al.*, Science **329**, 1500 (2010).
[6] K. R. Motes, A. Gilchrist, J. P. Dowling, and P. P. Rohde, Phys. Rev. Lett. **113**, 120501 (2014).
[7] S. Gross and M. J. Withford, Nanophotonics **4**, 332 (2015).
[8] M. Jachura, M. Karpiński, C. Radzewicz, and K. Banaszek, Opt. Express **22**, 8624 (2014).
[9] O. Gazzano, S. Michaelis de Vasconcellos, C. Arnold, A. Nowak, E. Galopin, I. Sagnes, L. Lanco, A. Lemaître, and P. Senellart, Nat. Commun. **4**, 1425 (2013).
[10] X. Ding *et al.*, Phys. Rev. Lett. **116**, 020401 (2016).
[11] A. J. Bennett, J. P. Lee, D. J. P. Ellis, T. Meany, E. Murray, F. F. Floether, J. P. Griffths, I. Farrer, D. A. Ritchie, and A. J. Shields, Sci. Adv. **2**, e1501256 (2016).
[12] T. Peyronel, O. Firstenberg, Q.-Y. Liang, S. Hofferberth, A. V. Gorshkov, T. Pohl, M. D. Lukin, and V. Vuletić, Nature (London) **488**, 57 (2012).
[13] F. Ripka, Y. H. Chen, R. Low, and T. Pfau, Phys. Rev. A **93**, 053429 (2016).
[14] O. Alibart, J. Fulconis, G. K. L. Wong, S. G. Murdoch, W. J. Wadsworth, and J. G. Rarity, New J. Phys. **8**, 67 (2006).
[15] A. B. U'Ren, C. Silberhorn, K. Banaszek, and I. A. Walmsley, Phys. Rev. Lett. **93**, 093601 (2004).
[16] M. A. Hall, J. B. Altepeter, and P. Kumar, Phys. Rev. Lett. **106**, 053901 (2011).
[17] X.-S. Ma, S. Zotter, J. Kofler, T. Jennewein, and A. Zeilinger, Phys. Rev. A **83**, 043814 (2011).
[18] X.-C. Yao, T.-X. Wang, P. Xu, H. Lu, G.-S. Pan, X.-H. Bao, C.-Z. Peng, C.-Y. Lu, Y.-A. Chen, and J.-W. Pan, Nat. Photonics **6**, 225 (2012).
[19] M. J. Collins *et al.*, Nat. Commun. **4**, 2582 (2013).
[20] S.-Y. Lan, A. G. Radnaev, O. A. Collins, D. N. Matsukevich, T. A. Kennedy, and A. Kuzmich, Opt. Express **17**, 13639 (2009).
[21] J. Nunn, N. K. Langford, W. S. Kolthammer, T. F. M. Champion, M. R. Sprague, P. S. Michelberger, X. M. Jin, D. G. England, and I. A. Walmsley, Phys. Rev. Lett. **110**, 133601 (2013).
[22] C. Simon, H. de Riedmatten, and M. Afzelius, Phys. Rev. A **82**, 010304 (2010).
[23] B. Albrecht, P. Farrera, G. Heinze, M. Cristiani, and H. de Riedmatten, Phys. Rev. Lett. **115**, 160501 (2015).
[24] A. Grodecka-Grad, E. Zeuthen, and A. S. Sørensen, Phys. Rev. Lett. **109**, 133601 (2012).
[25] P. S. Michelberger *et al.*, New J. Phys. **17**, 043006 (2015).
[26] C. H. van der Wal *et al.*, Science **301**, 196 (2003).
[27] K. F. Reim, P. Michelberger, K. C. Lee, J. Nunn, N. K. Langford, and I. A. Walmsley, Phys. Rev. Lett. **107**, 053603 (2011).
[28] M. Bashkansky, F. K. Fatemi, and I. Vurgaftman, Opt. Lett. **37**, 142 (2012).
[29] D. B. Higginbottom, B. M. Sparkes, M. Rancic, O. Pinel, M. Hosseini, P. K. Lam, and B. C. Buchler, Phys. Rev. A **86**, 023801 (2012).
[30] O. Firstenberg, M. Shuker, A. Ron, and N. Davidson, Rev. Mod. Phys. **85**, 941 (2013).
[31] H.-N. Dai *et al.*, Phys. Rev. Lett. **108**, 210501 (2012).
[32] M. Dąbrowski, R. Chrapkiewicz, and W. Wasilewski, Opt. Express **22**, 26076 (2014).
[33] See Supplemental Material at http://link.aps.org/supplemental/10.1103/PhysRevLett.118.063603 for the detailed discussion of multimode retrieval properties and heralding efficiency of presented holographic memory, which includes Refs. [34–40].
[34] D. G. England, K. A. G. Fisher, Jean-Philippe W. MacLean, P. J. Bustard, R. Lausten, K. J. Resch, and B. J. Sussman, Phys. Rev. Lett. **114**, 053602 (2015).
[35] P. J. Bustard, R. Lausten, D. G. England, and B. J. Sussman, Phys. Rev. Lett. **111**, 083901 (2013).
[36] M. Gündoğan, P. M. Ledingham, K. Kutluer, M. Mazzera, and H. de Riedmatten, Phys. Rev. Lett. **114**, 230501 (2015).
[37] D. J. Saunders, J. H. D. Munns, T. F. M. Champion, C. Qiu, K. T. Kaczmarek, E. Poem, P. M. Ledingham, I. A. Walmsley, and J. Nunn, Phys. Rev. Lett. **116**, 090501 (2016).
[38] M. D. Eisaman, A. André, F. Massou, M. Fleischhauer, A. S. Zibrov, and M. D. Lukin, Nature (London) **438**, 837 (2005).
[39] J. Kołodyński, J. Chwedeńczuk, and W. Wasilewski, Phys. Rev. A **86**, 013818 (2012).
[40] M. P. Edgar, D. S. Tasca, F. Izdebski, R. E. Warburton, J. Leach, M. Agnew, G. S. Buller, R. W. Boyd, and M. J. Padgett, Nat. Commun. **3**, 984 (2012).

[41] R. Chrapkiewicz and W. Wasilewski, Opt. Express **20**, 29540 (2012).
[42] M. Dąbrowski, R. Chrapkiewicz, and W. Wasilewski, J. Mod. Opt. **63**, 2029 (2016).
[43] M. Jachura and R. Chrapkiewicz, Opt. Lett. **40**, 1540 (2015).
[44] R. Chrapkiewicz, W. Wasilewski, and K. Banaszek, Opt. Lett. **39**, 5090 (2014).
[45] W. H. Peeters, J. J. Renema, and M. P. van Exter, Phys. Rev. A **79**, 043817 (2009).
[46] R. Chrapkiewicz, W. Wasilewski, and C. Radzewicz, Opt. Commun. **317**, 1 (2014).
[47] M. G. Raymer and J. Mostowski, Phys. Rev. A **24**, 1980 (1981).
[48] S. Manz, T. Fernholz, J. Schmiedmayer, and J. W. Pan, Phys. Rev. A **75**, 040101 (2007).
[49] T. Chanelière, D. N. Matsukevich, S. D. Jenkins, S.-Y. Lan, T. A. B. Kennedy, and A. Kuzmich, Nature (London) **438**, 833 (2005).
[50] X.-H. Bao, A. Reingruber, P. Dietrich, J. Rui, A. Dück, T. Strassel, L. Li, N.-L. Liu, B. Zhao, and J.-W. Pan, Nat. Phys. **8**, 517 (2012).
[51] P. Farrera, G. Heinze, B. Albrecht, M. Ho, M. Chávez, C. Teo, N. Sangouard, and H. de Riedmatten, Nat. Commun. **7**, 13556 (2016).
[52] D. N. Matsukevich, T. Chaneliere, S. D. Jenkins, S. Y. Lan, T. A. B. Kennedy, and A. Kuzmich, Phys. Rev. Lett. **97**, 013601 (2006).
[53] C.-W. Chou, J. Laurat, H. Deng, K. S. Choi, H. de Riedmatten, D. Felinto, and H. J. Kimble, Science **316**, 1316 (2007).
[54] D. E. Chang, V. Vuletić, and M. D. Lukin, Nat. Photonics **8**, 685 (2014).
[55] O. Jedrkiewicz, Y. K. Jiang, E. Brambilla, A. Gatti, M. Bache, L. A. Lugiato, and P. DiTrapani, Phys. Rev. Lett. **93**, 243601 (2004).
[56] V. Boyer, A. M. Marino, R. C. Pooser, and P. D. Lett, Science **321**, 544 (2008).